

Supporting Information for:

NiVO₃ Fused Oxide Nanoparticles – An Electrochemically Stable

Intercalation Anode Material for Lithium Ion Batteries

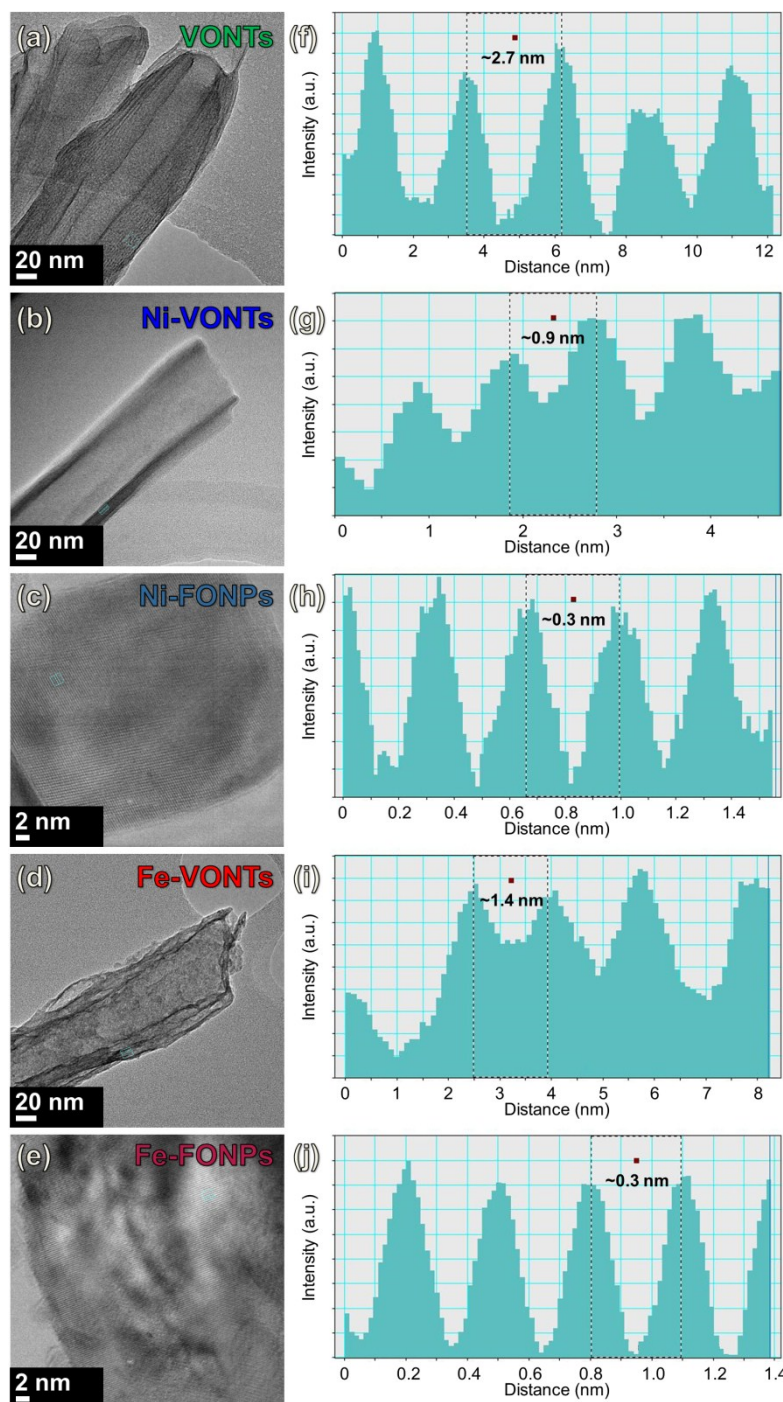


Fig. S1. TEM images of (a) as-prepared VONTs, (b) Ni-VONTs, (c) Ni-FONPs, (d) Fe-VONTs and (e) Fe-FONPs. Lattice spacings measured from TEM images using digital micrograph software for (f) as-prepared VONTs, (g) Ni-VONTs, (h) Ni-FONPs, (i) Fe-VONTs and (j) Fe-FONPs.

X-ray diffraction patterns for NiVO_3 phase are confirmed as the phase of the Ni-FONPS. Both NiVO_3 and a related triclinic CoVO_3 phase show very good agreement with the experimentally acquired pattern for Ni-FONPs. Relative intensity differences from certain planes exist likely between the nanoscale nature of the FONPs compared to the bulk crystal analysed in the original NiVO_3 studies, that were limited to ~ 56 degrees double angle. We find no other patterns that closely match the pattern apart from NiVO_3 , including other nickel vanadates such as $\text{Ni}_3\text{V}_2\text{O}_8$ (JCPDS 00-74-1484). We find no clear evidence that other isostructural compounds of different crystalline materials match the reference pattern, other than NiVO_3 .

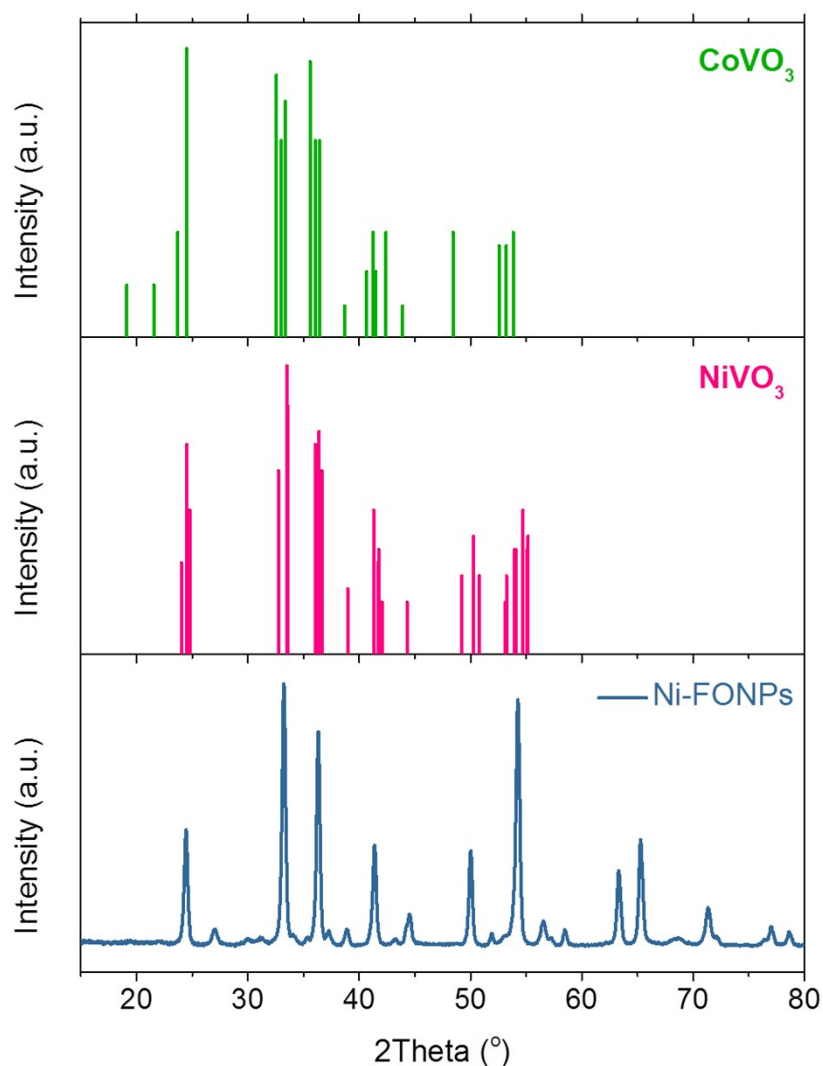


Fig. S2. XRD pattern for Ni-FONPs and reference stick patterns for NiVO_3 (JCPDS No. 00-027-1308) and CoVO_3 (JCPDS No. 00-026-0496).

SEM images of the ion-exchanged VONTs and heat treated FONPs are shown in Fig. S3. The tubular morphology of the Ni-VONTs and Fe-VONTs can be clearly seen in Fig. S3a

and d. The morphologies of the heat treated Ni-FONPs and Fe-FONPs are shown in Fig. S3b and e, respectively. FONPs are comprised of beaded rods of fused nanoparticles as can be seen the SEM images. SEM images of Ni-FONPs and Fe-FONPs after 500 galvanostatic cycles, with an applied specific current of 200 mA/g are shown in Fig. S3c and f, respectively. Energy-dispersive X-ray spectroscopy (EDS) spectra for ion exchanged VONTs, as-prepared FONPs samples and FONP samples after 500 galvanostatic cycles were acquired over the areas shown in the SEM images in Fig. S3a-f. The presence of peaks attributed to the presence of Ni can be seen in the spectra for Ni-VONTs and Ni-FONPs, before and after cycling. The relative amounts of each element present in the samples are listed in Table 1.

Table S1. Atomic % of elements present from EDS measurements.

Element	Atomic %					
	Ni-VONTs	Ni-FONPs	Ni-FONPs after 500 cycles	Fe-VONTs	Fe-FONPs	Fe-FONPs after 500 cycles
V	27.93	24.74	12.60	25.24	26.95	6.38
O	54.48	43.88	56.87	49.41	41.93	56.94
Fe	-	-	-	14.43	19.45	5.40
Ni	5.95	19.75	3.83	-	-	-
C	10.06	11.63	18.55	9.78	11.67	20.94
Cl	1.58	-	0.29	1.14	-	1.18
Si	-	-	0.34	-	-	0.40
P	-	-	1.45	-	-	1.01
F	-	-	6.07	-	-	7.75

The spectra for the Fe-VONTs and Fe-FONPs confirm the presence of Fe, V, O and C within the structure. The characteristic C peak at ~ 0.27 keV is likely due to presence of the hydrocarbon chain of any amine molecules remaining after the ion exchange reaction in the case of the Ni and Fe-VONTs and the thermal decomposition of amines in the case of the FONP samples, as well as adventitious carbon on the surface of the nanostructures. A low

intensity peaks associated with Cl is present due to Cl based precursors which were used as a source of both Fe and Ni ions. However, traces of Cl were not observed in the EDS spectra for the heated FONP samples.

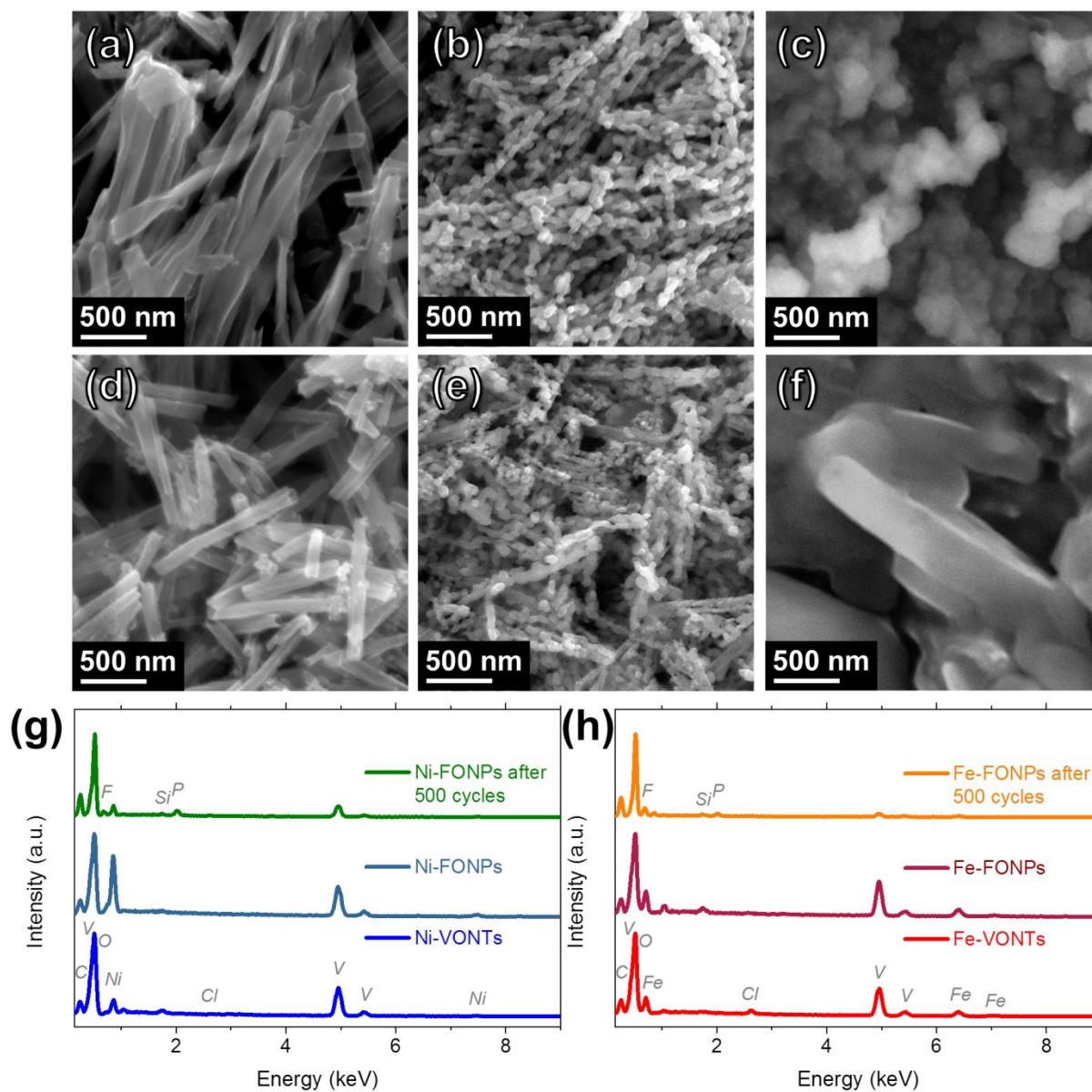


Fig. S3. SEM images of (a) Ni-VONTs, (b) Ni-FONPs, (c) Fe-VONTs and (d) Fe-FONPs. (e) EDS spectra for ion-exchanged VONT and heated FONP samples acquired from the areas shown in (a)-(d).

Ni and Fe-FONP samples after electrochemical testing contained traces of Si, P and F which were not observed in the spectra for the ion exchanged VONT samples or the FONP samples prior to electrochemical testing. The Si observed is due to the glass fibre separator which was used for all electrochemical tests, and P and F are present from the electrolyte

which was used (a 1 mol dm⁻³ solution of LiPF₆ in a 1:1 (v/v) mixture of ethylene carbonate in dimethyl carbonate with 3 wt% vinylene carbonate).

Elemental maps were acquired from scanning transmission electron microscope energy-dispersive X-ray spectroscopy in order to determine the distribution of each element present in Ni-FONPs and Fe-FONPs, as shown in Fig. S4. It can be seen from the elemental maps that Ni, V and O are homogeneously distributed within the Ni-FONPs. Likewise, Fe, V and O are also homogeneously distributed within the Fe-FONPs.

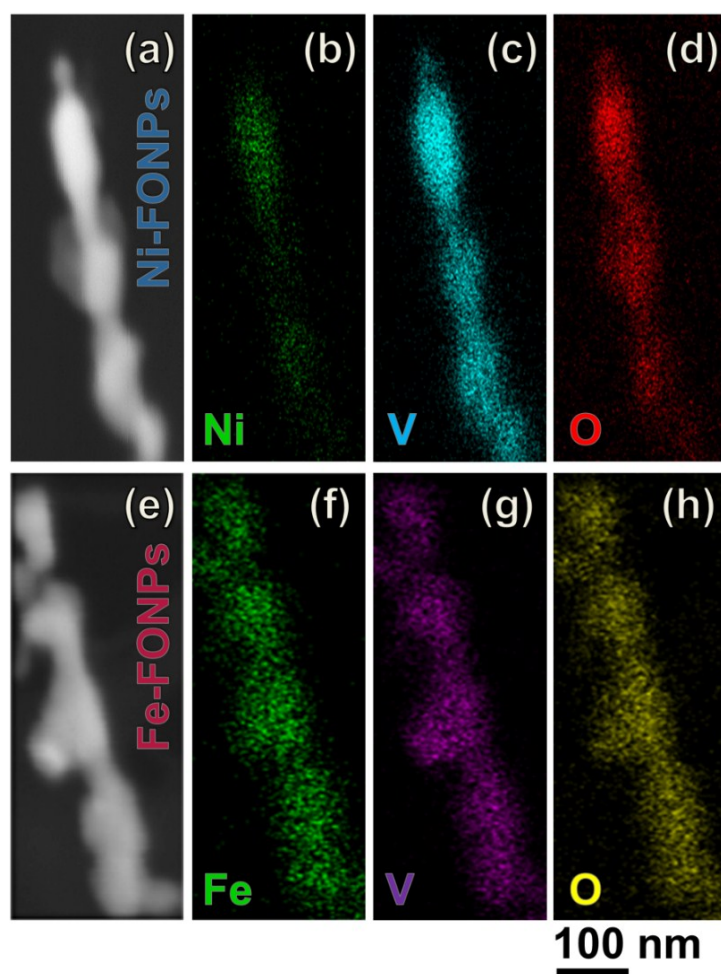


Fig. S4. Scanning transmission electron microscope (STEM) energy-dispersive X-ray spectroscopy (EDS) elemental maps for Ni-FONPs and Fe-FONPs illustrating the distribution of each element present.

Table S2. XPS binding energies for fitted peaks (in eV). The relative amounts of each vanadium oxidation state are shown in parentheses

Sample	Fe 2p _{3/2}		Ni 2p _{3/2}		V 2p _{3/2}		O 1s
	Fe ³⁺	Fe ²⁺	Ni ³⁺	Ni ²⁺	V ⁵⁺	V ⁴⁺	
Fe-VONTs	710.57 (37%)	712.19 (63%)	-	-	517.24 (91%)	515.77 (9%)	530.19
Fe-FONPs	710.89 (35%)	712.38 (65%)	-	-	517.30 (80%)	515.68 (20%)	530.11
Ni-VONTs	-	-	856.54 (72%)	855.75 (28%)	517.25 (88%)	515.82 (12%)	530.15
Ni-FONPs	-	-	857.43 (34%)	855.99 (66%)	517.27 (88%)	515.84 (12%)	530.17

The high resolution spectra for the O 1s region for all samples, contained three oxygen contributions, as shown in Fig. S5. The peak at ~ 530.2 eV is archetypal of metal-oxygen bonds.^{1,2} The peak at ~ 531.4 eV can be assigned to defects and a number of surface species including hydroxyls, chemisorbed oxygen or under-coordinated lattice oxygen.^{3,4} The peak present at ~ 533.3 eV can be attributed to multiplicity of physi- and chemisorbed water at or near the surface.^{1,2}

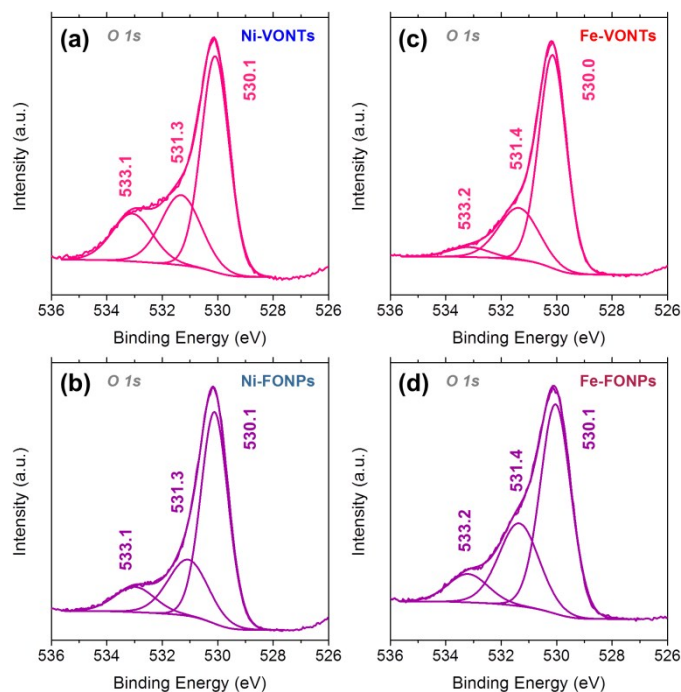


Fig. S5. XPS spectra of the O 1s regions for (a) Ni-VONTs, (b) Ni-FONPs, (c) Fe-VONTs and (d) Fe-FONPs

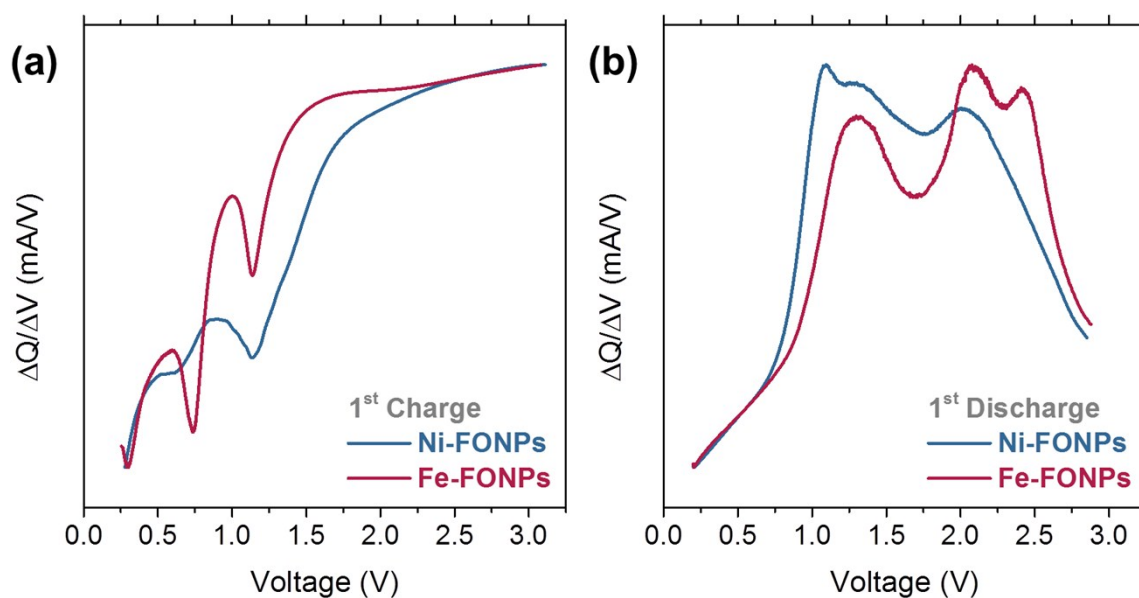


Fig. S6. Differential capacity plots calculated from (a) the first charge and (b) the first discharge voltage profiles for Ni-FONPs and Fe-FONPs, cycled galvanostatically using a specific current of 200 mA/g.

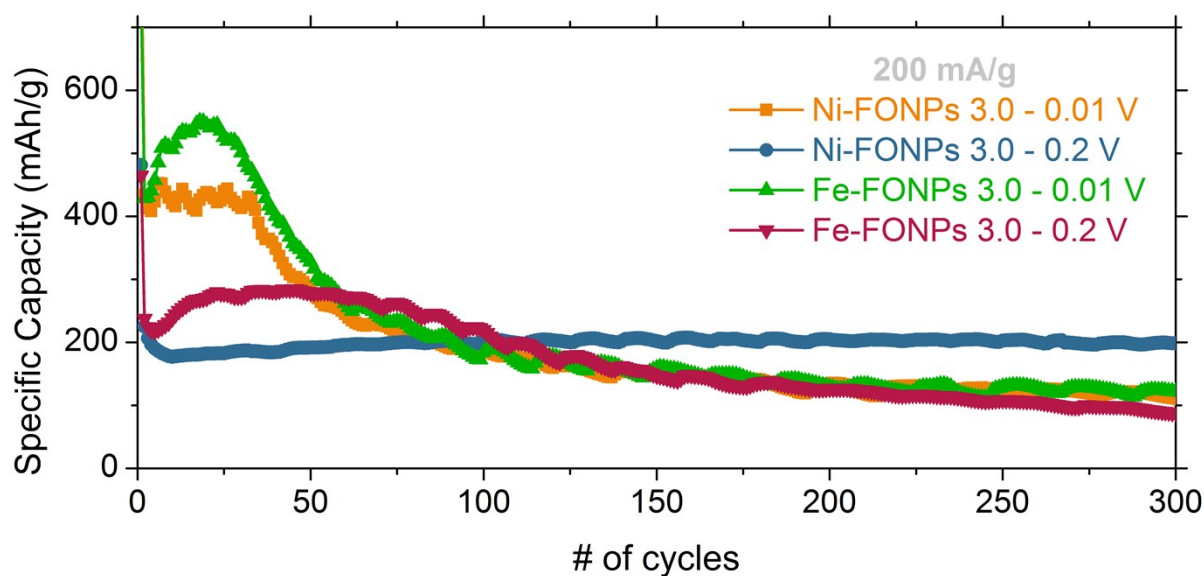


Fig. S7. Comparison of the specific capacity values obtained for Ni-FONPs and Fe-FONPs over 500 cycles in potential windows of 3.0 – 0.01 V and 3.0 – 0.2 V with an applied specific current of 200 mA/g.

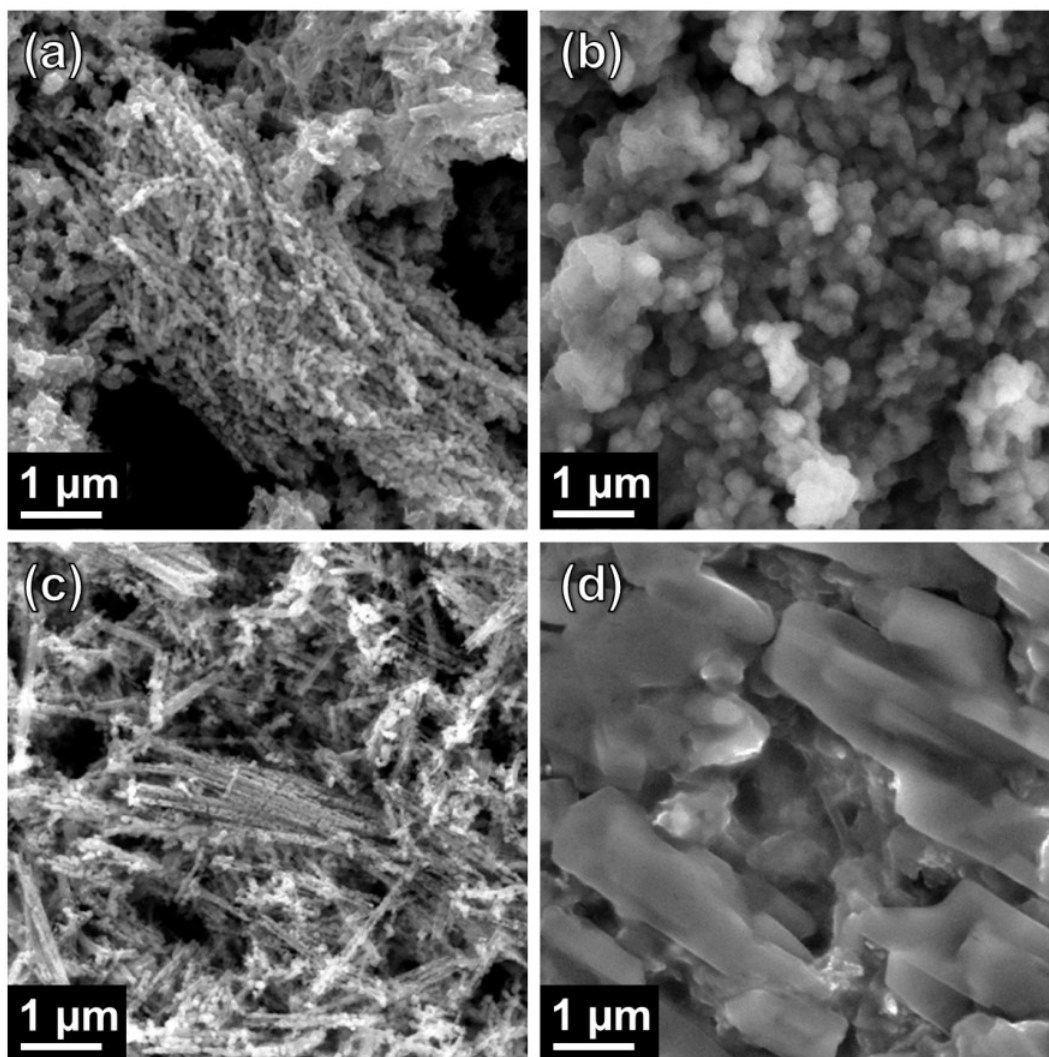


Fig. S8. SEM images of Ni-FONPs (a) before and (b) after 500 galvanostatic cycles and Fe-FONPs (c) before and (d) after 500 galvanostatic cycles using an applied specific current of 200 mA/g. The Fe_2O_3 and V_2O_3 nanocomposite material appears coated with the Li_2O phase, completely absent in the NiVO_3 cycled anode material. Note: All images were acquired at the same magnification (20,000 \times).

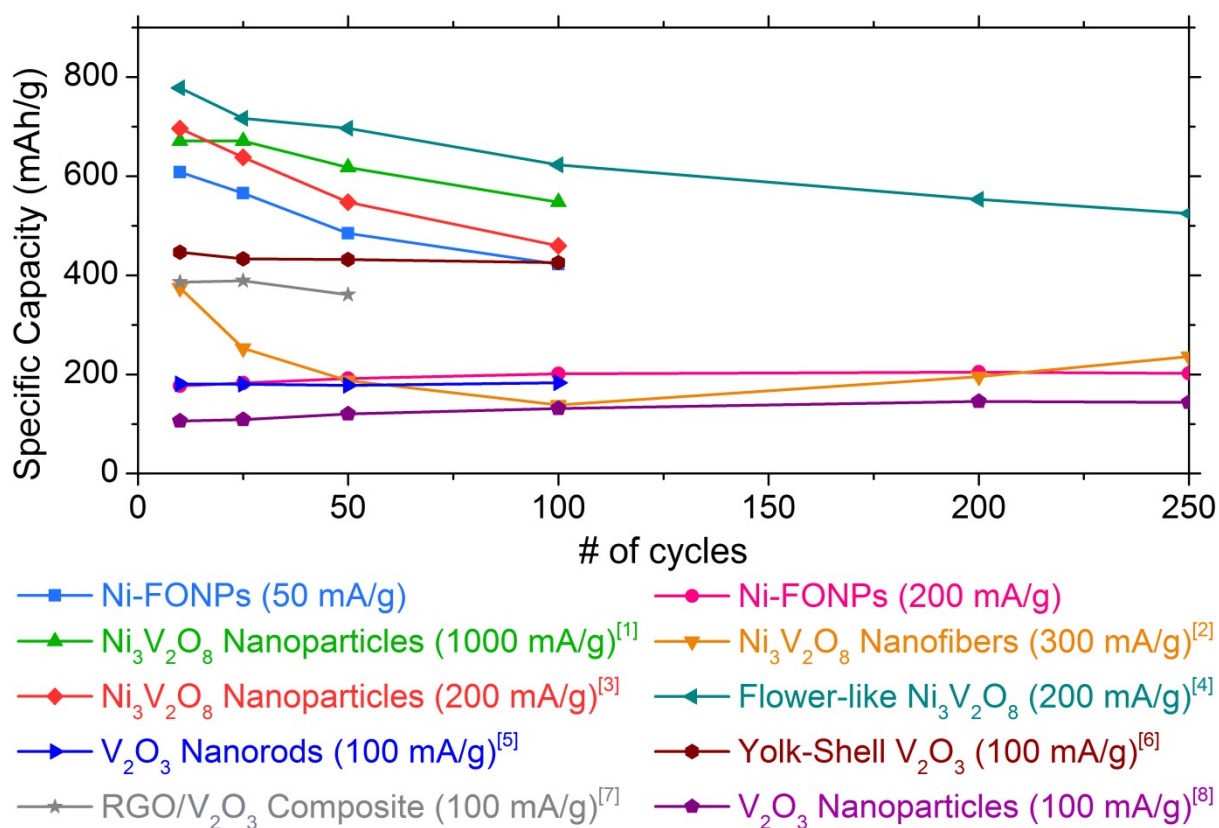


Fig. S9. Comparison of reported specific capacity values for Ni₃V₂O₈ and V₂O₃ nanostructures from the literature: Ni₃V₂O₈ nanoparticles⁵, Ni₃V₂O₈ nanofibers⁶, Ni₃V₂O₈ nanoparticles⁷, flower-like Ni₃V₂O₈⁸, V₂O₃ nanorods⁹, yolk-shell V₂O₃¹⁰, RGO/ V₂O₃ composite¹¹, V₂O₃ nanoparticles¹².

Table S3. Comparison of capacities obtained for various Ni₃V₂O₈ and V₂O₃ nanostructures from the literature

Material	C-rate	Charge Capacity mAh/g						Ref.
		10th	25th	50th	100th	200th	250th	
Ni-FONPs	50 mA/g	607.9	565.9	484.6	422.6	-	-	This work
Ni-FONPs	200 mA/g	177.2	182.7	191.8	201.3	204.7	202.5	This work
Ni ₃ V ₂ O ₈ Nanoparticles	1000 mA/g	670.8	670.7	617.7	547.8	-	-	1
Ni ₃ V ₂ O ₈ Nanofibers	300 mA/g	375.0	252.7	187.5	138.6	195.7	236.4	2
Ni ₃ V ₂ O ₈ Nanoparticles	200 mA/g	696.4	638.0	547.4	459.7	-	-	3
Flower-like Ni ₃ V ₂ O ₈	200 mA/g	778.2	716.9	696.5	622.9	553.4	524.8	4
V ₂ O ₃ nanorods	100 mA/g	180.9	180.3	178.3	183.6	-	-	5
Yolk-Shell V ₂ O ₃ Microspheres	100 mA/g	446.8	433.3	431.8	425.8	-	-	6
RGO/V ₂ O ₃ Composite	100 mA/g	386.0	388.8	360.8	-	-	-	7
V ₂ O ₃ nanoparticles	100 mA/g	106.2	109.2	120.3	131.4	145.5	143.6	8

References:

- (1) Marco, J. F.; Gancedo, J. R.; Gracia, M.; Gautier, J. L.; Ríos, E.; Berry, F. J., Characterization of the Nickel Cobaltite, NiCo_2O_4 , Prepared by Several Methods: An XRD, XANES, EXAFS, and XPS Study. *J. Solid State Chem.* **2000**, *153*, 74-81.
- (2) Choudhury, T.; Saied, S. O.; Sullivan, J. L.; Abbot, A. M., Reduction of oxides of iron, cobalt, titanium and niobium by low-energy ion bombardment. *J. Phys. D* **1989**, *22*, 1185.
- (3) Roginskaya, Y. E.; Morozova, O. V.; Lubnin, E. N.; Ulitina, Y. E.; Lopukhova, G. V.; Trasatti, S., Characterization of Bulk and Surface Composition of $\text{Co}_x\text{Ni}_{1-x}\text{O}_y$ Mixed Oxides for Electrocatalysis. *Langmuir* **1997**, *13*, 4621-4627.
- (4) Zhong, J.-H.; Wang, A.-L.; Li, G.-R.; Wang, J.-W.; Ou, Y.-N.; Tong, Y.-X., $\text{Co}_3\text{O}_4/\text{Ni}(\text{OH})_2$ composite mesoporous nanosheet networks as a promising electrode for supercapacitor applications. *J. Mater. Chem.* **2012**, *22*, 5656-5665.
- (5) Sambandam, B.; Soundharrajan, V.; Song, J.; Kim, S.; Jo, J.; Pham, D. T.; Kim, S.; Mathew, V.; Kim, K. H.; Sun, Y.-K.; Kim, J., $\text{Ni}_3\text{V}_2\text{O}_8$ nanoparticles as an excellent anode material for high-energy lithium-ion batteries. *J. Electroanal. Chem.* **2018**, *810*, 34-40.
- (6) Lv, C.; Sun, J.; Chen, G.; Yan, C.; Chen, D., Achieving $\text{Ni}_3\text{V}_2\text{O}_8$ amorphous wire encapsulated in crystalline tube nanostructure as anode materials for lithium ion batteries. *Nano Energy* **2017**, *33*, 138-145.
- (7) Soundharrajan, V.; Sambandam, B.; Song, J.; Kim, S.; Jo, J.; Pham, D. T.; Kim, S.; Mathew, V.; Kim, J., Bitter gourd-shaped $\text{Ni}_3\text{V}_2\text{O}_8$ anode developed by a one-pot metal-organic framework-combustion technique for advanced Li-ion batteries. *Ceramics International* **2017**, *43*, 13224-13232.
- (8) Li, Y.; Kong, L.-B.; Liu, M.-C.; Zhang, W.-B.; Kang, L., One-step synthesis of micro/nano flower-like $\text{Ni}_3\text{V}_2\text{O}_8$ as anode for Li-ion batteries. *Mater. Lett.* **2017**, *186*, 289-292.
- (9) Li, X.; Fu, J.; Pan, Z.; Su, J.; Xu, J.; Gao, B.; Peng, X.; Wang, L.; Zhang, X.; Chu, P. K., Peapod-like V_2O_3 Nanorods Encapsulated into Carbon as Binder-free and Flexible Electrodes in Lithium-ion Batteries. *J. Power Sources* **2016**, *331*, 58-66.
- (10) Jiang, L.; Qu, Y.; Ren, Z.; Yu, P.; Zhao, D.; Zhou, W.; Wang, L.; Fu, H., In Situ Carbon-Coated Yolk-Shell V_2O_3 Microspheres for Lithium-Ion Batteries. *ACS Appl. Mater. Interfaces* **2015**, *7*, 1595-1601.
- (11) Zhang, Y.; Pan, A.; Liang, S.; Chen, T.; Tang, Y.; Tan, X., Reduced graphene oxide modified V_2O_3 with enhanced performance for lithium-ion battery. *Mater. Lett.* **2014**, *137*, 174-177.
- (12) Song, H. J.; Choi, M.; Kim, J.-C.; Park, S.; Lee, C. W.; Hong, S.-H.; Kim, D.-W., Li-electroactivity of thermally-reduced V_2O_3 nanoparticles. *Mater. Lett.* **2016**, *180*, 243-246.